Philippe Schaffnit[a], Charles Stallybrass[a], Joachim Konrad[a], Axel Kulgemeyer[a], Heike Meuser[b]
[a] Salzgitter Mannesmann Forschung GmbH, Duisburg, Germany
[b] Salzgitter Mannesmann Grobblech GmbH, Mülheim an der Ruhr, Germany

Dual-scale phase-field simulation of grain growth upon reheating of a microalloyed line pipe steel

The austenite grain growth of a microalloyed steel was investigated via annealing experiments and phase-field simulations using the phase-field code Micress. The technique described in a previous work was enhanced and applied to an Nb, Ti microalloyed linepipe steel for the case of isothermal heat treatment between 1 050 and 1 200 °C. The input parameters for the phase-field simulations were deduced from physical models based on the results of isothermal holding experiments. A further improvement was the use of the software package MatCalc to simulate at a lower scale the coarsening of the pinning particles. The results of these simulations showed good agreement with the experimental results.

Keywords: Linepipe; Modelling; Grain growth; Phase-field; Particle pinning

1. Introduction

Thermomechanically treated microalloyed steels are widely used for linepipe applications because of their attractive combination of high strength, high low-temperature toughness and excellent weldability. A key factor for achieving these properties lies in the control of the grain size in all stages of production from thermomechanical processing to welding. This is strongly influenced by the microalloying elements, see for example [1]. Knowledge of the effect of an exposure to high temperatures on the grain size is required in order to define a feasible production window.

The austenite grain growth during reheating of a microalloyed steel in the temperature range from 1 050 °C to 1 200 °C was investigated both experimentally and by simulations based on the phase-field method. Isothermal annealing experiments were carried out in order to investigate the grain growth kinetics. Simulations were performed using the phase-field code Micress [2].

In pure metals, grain growth kinetics follow a parabolic growth law. Especially in the case of microalloyed steels, however, it is necessary to take the pinning effect of second phase particles into account in order to obtain agreement with the experimental results. The technique described in a previous work [3] was used to deduce the input parameters for the phase-field simulations from physical models based on the results of isothermal holding experiments. Several models were tested: the second phase particles were first assumed to remain unchanged over the annealing time, then to undergo an Ostwald ripening process and the software package MatCalc [4] was used to simulate explicitly at a lower scale the coarsening of the pinning particles. The robustness of this model was tested using the input data derived from the experiments at 1 050 °C and 1 200 °C to simulate the annealing experiments at 1 100 °C and 1 150 °C.

2. Models

2.1. Multi-phase-field

The simulations were performed using the Micress code implementing the multi-phase-field model [5]. The multi-phase-field description is based on the so-called order parameter conveying the local fraction of each individual grain: for grain i, $\varphi_i = 1$ in its bulk, $\varphi_i = 0$ where it is not present, and in a binary interface between grains i and j, $\varphi_i + \varphi_j = 1$. The space is filled when $\sum_{i=0}^{N} \varphi_i = 1$ is met (where N is the total number of grains). In the case of grain growth, the only driving force is the minimisation of the surface energy, and the equation to be solved can be simplified as:

$$\dot{\varphi}_i = \sum_{j=1}^{N} \mu_{ij}\sigma_{ij}\left[(\varphi_j\nabla^2\varphi_i - \varphi_i\nabla^2\varphi_j) + \frac{\pi^2}{2\eta^2}(\varphi_i - \varphi_j)\right] \qquad (1)$$

Where η is the grid-spacing and $\mu \times \sigma$ the kinetic coefficient: product of the surface energy and the interface mobility.

2.2. Effective mobility

The particle pinning model [6] implemented in Micress uses an effective interface mobility [7] as in Eq. (2), where Γ is the local mean curvature of the grain boundary, Γ_Z a critical curvature, $\mu_{\min}$ minimum mobility (introduced for numerical stability purposes) is here set to one thousandth of the pre-exponential factor μ_0. This formulation has the additional benefit of dissociating completely the pinning parameters from the surface energy (which would be necessary, were it to be expressed in terms of pressure).

$$\mu = \mu_0 \times \exp\left(\frac{1}{1 - \frac{\Gamma}{\Gamma_Z}}\right) \quad \text{and} \quad \mu \geq \mu_{\min} \qquad (2)$$

2.3. Ostwald ripening of the pinning particles

The critical curvature was first assumed to depend only on the temperature, but the model developed by Militzer [8], where the pinning particles are assumed to undergo Ostwald ripening was also used, simplified as Eq. (3). The term accounting for a possible residual critical curvature was neglected as the ripening process has not reached a stage where it could be significant, and the two remaining parameters can then readily be derived from the linear interpolation performed on the experimental data. Γ_Z is the critical curvature, Γ_{Z_0} the initial critical curvature and τ a characteristic time for the ripening kinetics.

$$\Gamma_Z = \frac{\Gamma_{Z_0}}{\left(1 + \frac{t}{\tau}\right)^{1/3}} \tag{3}$$

2.4. Explicit simulation of the ripening of the pinning particles

The Zener equation relates the critical curvature Γ_Z to the phase fraction of the second phase particles f and their average radius $\langle r \rangle$ via a constant K (see for example [6]). The software package MatCalc can calculate the fraction of second phases as well as the average particle size, leaving the critical curvature and K as the only unknown in Eq. (4). The critical curvature derived from MatCalc is then input in Micress as a function of time.

$$\Gamma_Z = \frac{1}{K}\frac{f}{\langle r \rangle} \tag{4}$$

3. Experiments

3.1. Experimental procedure

In order to investigate the kinetics of austenite grain growth, annealing experiments were carried out. Specimens with dimensions of 15 × 15 × 10 mm were taken from continuous cast material and subjected to heat treatments in an inert atmosphere. The samples were held at temperatures between 1 050 °C and 1 200 °C and quenched after isothermal holding for 1 min to 300 min.

The pipeline steel used was microalloyed with Nb and Ti. The temperature was controlled by thermocouples that were attached to the specimen in the centre. After holding, the cross-section of the specimens corresponding to the position of the thermocouples was prepared for metallographic investigation by annealing well below the A_{c1} temperature and etching with a solution of picric acid. Examples of the evolution of the austenite grain size are shown in Fig. 1. The grain size was determined using the linear intercept method.

3.2. Assessment of experimental results

The grain ensemble was described via the median, lower and upper quartiles (cutting off the 25 % smallest and largest grains of the grain size distribution respectively), rather than its average and standard deviation. Indeed, if a distribution is markedly non-symmetric, as in this case, the average can get significantly skewed. Figure 2 is a so-called 'violin plot' of the grain size distribution after 300 min holding at 1 050, 1 100, 1 150 and 1 200 °C, that also shows the width and the shape of the distribution, illustrating that the distributions are indeed non-symmetric.

Figure 3 shows the evolution of the median grain radius over time. As the two non linear scales for the time show,

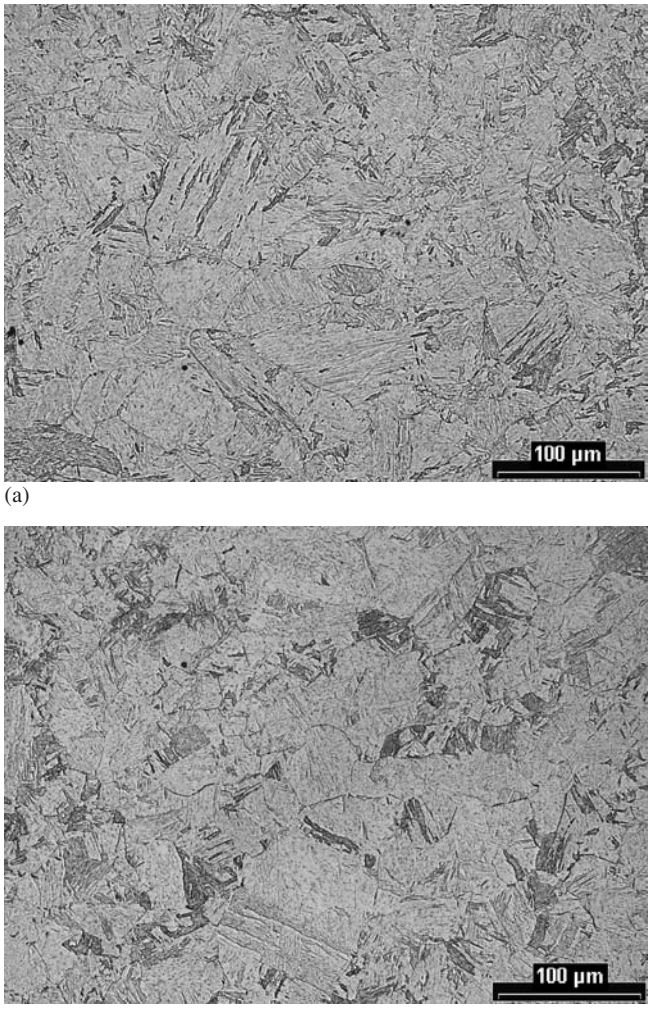

(a)

(b)

Fig. 1. Experimental micrographs after holding at 1 200 °C. (a): After 1 min; (b): After 100 min.

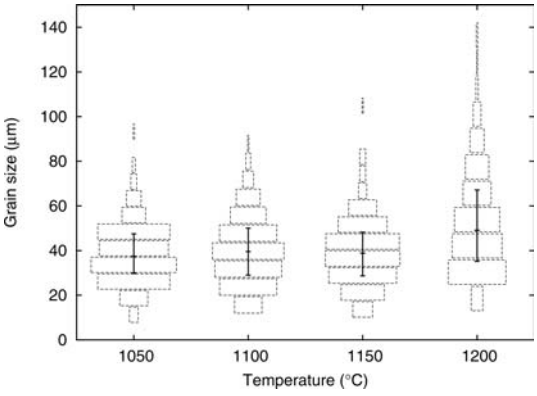

Fig. 2. Grain size distribution, as well as the median, first and third quartiles after 300 min holding.

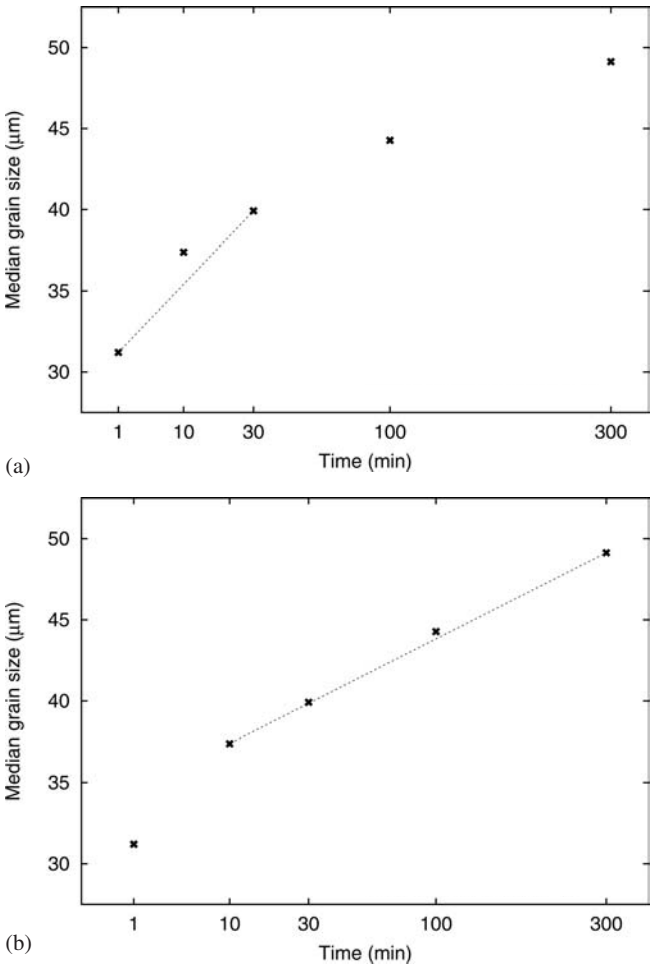

Fig. 3. Median grain size for isothermal holding at 1 200 °C. (a): Quadratic time scale ("$\langle R\rangle$ ($\sqrt{t}$)"); (b): Cubic time scale ("$\langle R\rangle$ ($\sqrt[3]{t}$)").

two regimes can be distinguished: up to 30 min, the growth can be considered to be quadratic, which is attributed to unhindered grain-growth, Eq. (6). From 10 min on, the behaviour is cubic, consistent with the Militzer model [8], Eq. (3).

$$\langle R\rangle^2(t) = \langle R\rangle^2(t_0) + \left(8 \times \frac{R}{\rho}\right) \times \sigma \times \mu \times t \qquad (5)$$

Hillert [9] derived Eq. (5) where ρ is the mean principal curvature radius of the interface, and R the grain size. If the geometry factor $8 \times \frac{R}{\rho}$ is assumed to be constant ($\frac{R}{\rho} = 10$ here), the kinetic constant $\sigma \times \mu$ ($\sigma \times \mu_0$ in the Micress description) is the only unknown in Eq. (5). It was calculated according to the regression made on the experimental data for the parabolic regime at the beginning of the holding when the effect of particle-pinning on the growth kinetics is weakest (cf. Fig. 3a). As can be seen in Fig. 4, the kinetic factor roughly follows an Arrhenius law.

If the grains are assumed to have reached their critical size (and if as previously $\frac{R}{\rho}$ is constant), the critical curvature can be calculated from the median grain size: $\Gamma_Z(t) = \frac{2}{\rho(t)} = 2 \times \frac{R}{\rho} \times \frac{1}{R(t)}$. The time constant and factor of Eq. (3) can then be calculated from the regression performed on Fig. 3b.

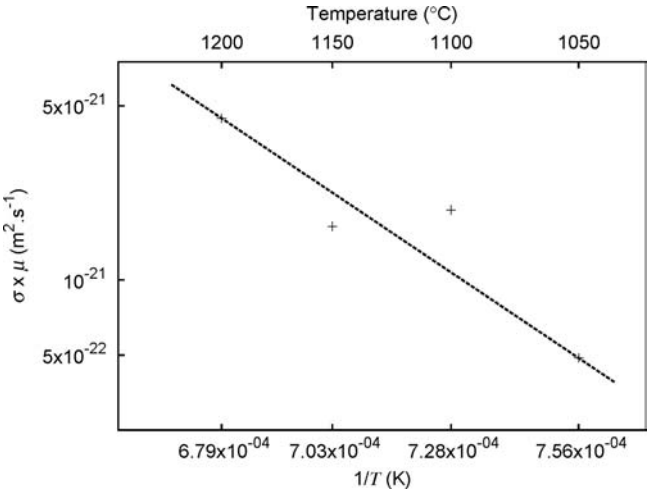

Fig. 4. Kinetic factor as a function of the temperature.

Table 1. Zener factor as a function of temperature.

T(°C)	1 050	1 100	1 150	1 200
K	3.02	3.00	2.80	3.51

The results of a simulation mirroring closely the production of the slabs was taken as the initial state for the MatCalc annealing simulations. The average particle size and phase fraction calculated with MatCalc were combined with the experimentally derived critical curvature after 300 min according to Eq. (4) to evaluate the Zener constant K. The corresponding values for all holding temperatures are shown in Table 1.

4. Simulations

4.1. Ideal grain growth

The quality of the set-up (namely the initial grain size distribution and the spatial discretisation) was assessed by running ideal grain-growth simulations, the results of which were compared with theoretical references.

This process is only detailed for the simulation related to the annealing at 1 200 °C, where 5 000 grains in a 2 768 × 2 768 domain evolved into 195 grains over 94 196 time-steps.

The initial microstructures for the simulations were set according to a weighted Voronoi construct. The nodes were set on a hexagonal grid with white noise (with an amplitude of half of the distance between nearest neighbours), and the weight was chosen as a log-normal distribution. The boundary effects at the edge of the domain do not need to be taken into account, as periodic (wrap-around) conditions were used.

Figure 5 shows the evolution of the average grain radius over time (as well as the number of remaining grains). The data were fitted with a least-squares method using Eq. (6), where $t_0 = 0$. The resulting growth rate exponent m was 0.53 which agrees quite well with the theoretical prediction of $\frac{1}{2}$ [10].

$$\langle R\rangle(t) = \langle R\rangle(t_0) + k \times (t - t_0)^m \qquad (6)$$

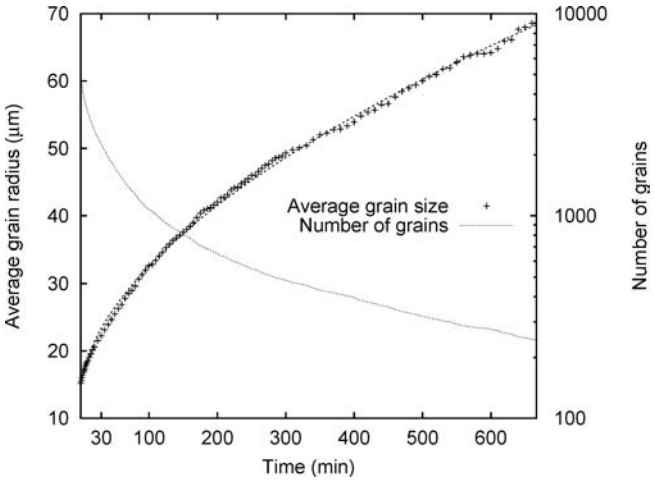

Fig. 5. Average grain radius over time for the ideal grain-growth simulation at 1 200 °C.

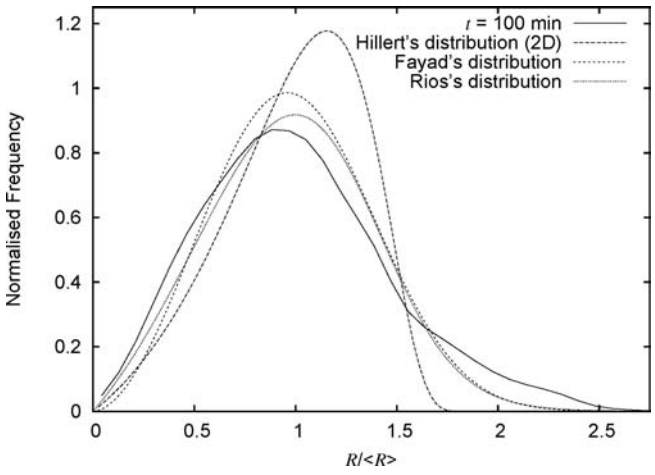

Fig. 7. Normalised reduced grain size distributions (simulation at 1 200 °C of ideal grain-growth), in combination with the distributions according to Hillert, Fayad and Rios.

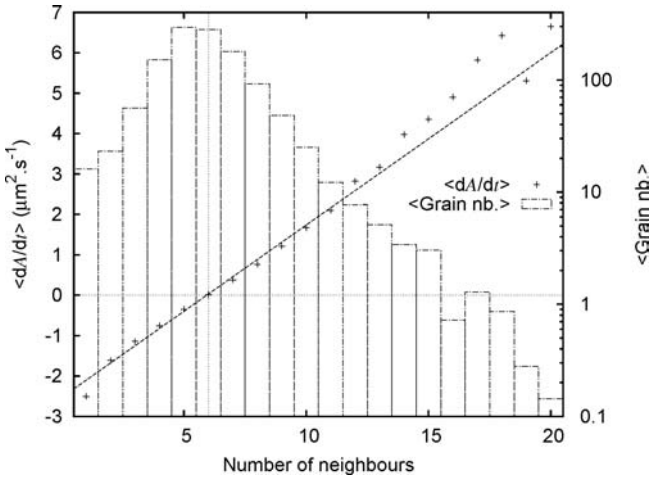

Fig. 6. Derivative of a grain's surface versus its number of neighbours (classes population on second scale), ideal grain-growth simulation at 1200 °C.

According to the von Neumann–Mullins relation, the growth rate of a grain is proportional to its number of sides [11], see Eq. (7), where A is the area of a grain, σ the surface energy, μ the interface mobility and n the number of sides. The number of neighbours of a grain was used as a proxy for its number of sides. The grains were sorted into classes according to their number of neighbours and for each class the derivative of the surface was averaged over the whole simulation, see Fig. 6. The data were fitted with a least-squares method weighted with the class population. The correlation coefficient was 0.992, and the predicted "stable configuration" was 5.93 neighbours, which is in accordance with theory [11], as the stable configuration in 2D is that of hexagonal grains. The slope of the linear regression is $0.445\ \mu\mathrm{m}\cdot\mathrm{s}^{-1}$ whereas $\sigma\times\mu\times\frac{\pi}{3}=0.466\,\mu\mathrm{m}\cdot\mathrm{s}^{-1}$. The non-linearity for fourteen and more neighbours can be discounted as these configurations are only briefly present during the initial transient.

$$\frac{\mathrm{d}A}{\mathrm{d}t}=\sigma\times\mu\times\frac{\pi}{3}\times(n-6) \tag{7}$$

Finally, the grain size distribution was compared to the Hillert distribution (an analytical distribution derived from a mean-field theory consistent with a parabolic growth law [9]), as well as a Weibull distribution suggested by Fayad et al. [12, 13] and another proposed by Rios [13]. Poor agreement with the Hillert distribution has been consistently reported [13, 14]. Nevertheless, it provides a convenient reference: the plateau towards higher grain radii has also been observed by [14]. As can be seen on Fig. 7, the agreement with the Rios distributions is fair.

Unlike in [3], the three-dimensional ideal grain-growth simulations did not agree well enough with the theoretical results and are not shown here. The growth exponent was found to be 0.69, compared to a theoretical value of 0.5. The observed stable configuration found was 17.05 neighbours as opposed to the expected 13.397. Finally, the grain size distribution did not become self-similar. In [3] the typical grain size allowed for finer spatial discretisation than in the present case. The log-normal grain size distribution used here calls for more grains to be adequately defined (a Gaussian distribution was used in [3]). Improved results are expected when more grains are taken into account and the grid-spacing is decreased. This is currently difficult as both increase the memory usage which is already at the limit of what is addressable by the current commercial Micress executables. This issue will be addressed in the near future by switching to 64-bit binaries.

On the other hand, the set-up of the two-dimensional simulations were successfully validated for ideal grain-growth and could therefore be used with confidence for particle-pinning simulations. Two-dimensional approximations of three-dimensional processes are frequently carried out when three-dimensional simulations cannot be made because of inadequate computing power (see for example, [15]).

4.2. Annealing simulations at 1 200 °C

Figure 8 shows the evolution of the median, first and third quartiles of the grain size grain radius over time for the following models: no particle pinning (as a reference), no ripening of precipitates (critical curvature derived from the

grain size after 300 min annealing), the Militzer model (τ and Γ_{Z_0} deduced from the 'cubic' regime, as detailed in Section 3.2). The simulation without particle pinning clearly leads to too large a grain size (Fig. 8a). Not taking into account the coarsening of the pinning particles overestimates the effect of grain growth (Fig. 8b). The Militzer model as well as the MatCalc-based simulation take into account the effect on the critical curvature of coarsening of the pinning particle, which is then input in Micress as time-dependent. The Militzer model assumes Ostwald ripening of the particles, whereas MatCalc implements a numerical Kampann–Wagner model. The Militzer model offers a very nice match (Fig. 8c). The MatCalc-based simulation (Fig. 8d) predicts a slightly too low first quartile up to 30 min, which might be a hint that the initial grain structure could be further improved (as this can also be ob-

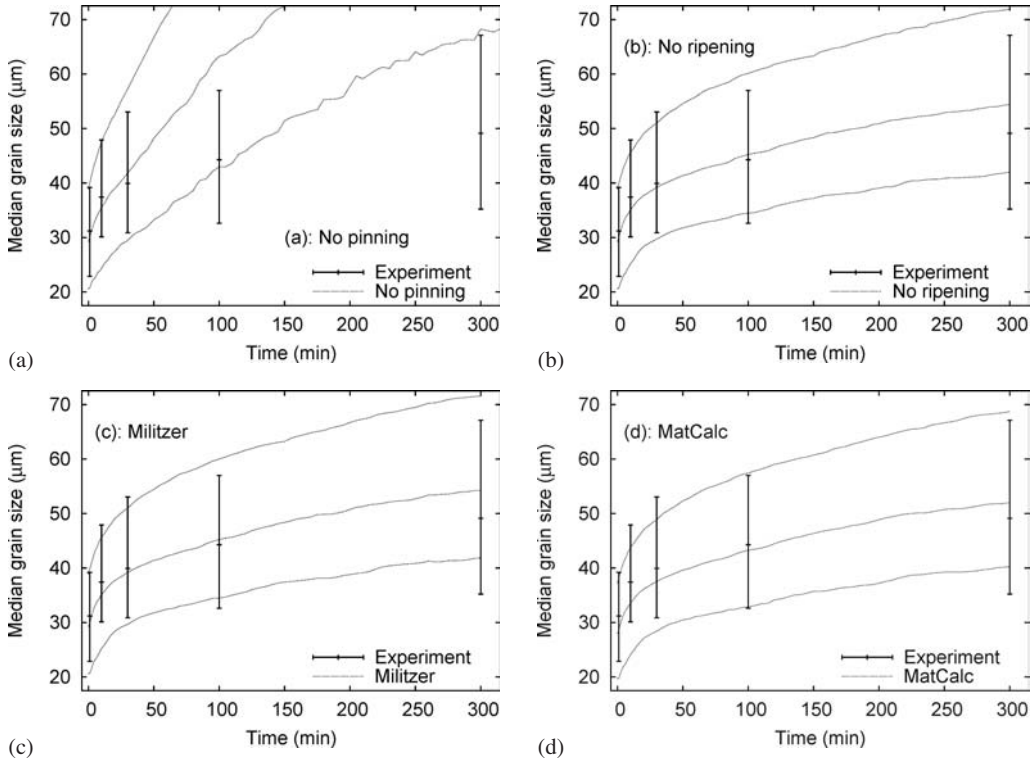

Fig. 8. Evolution of the median, first and third quartiles of the grain size distribution by annealing at 1200 °C. (a): No pinning; (b): No ripening; (c): Militzer; (d): MatCalc.

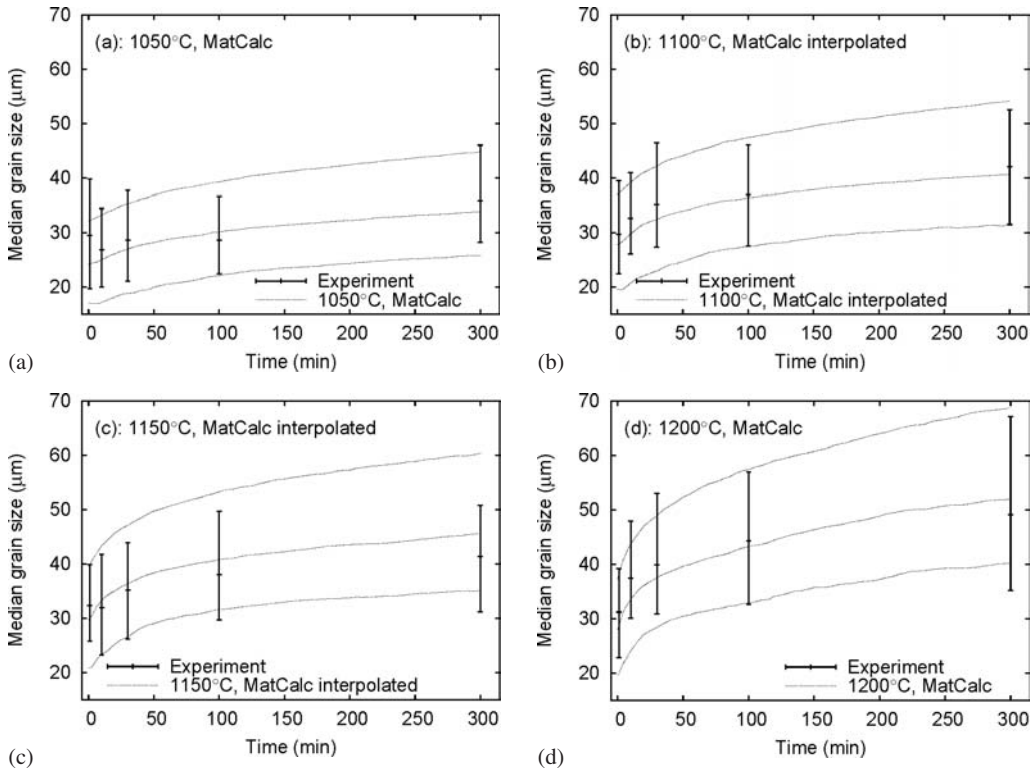

Fig. 9. Evolution of the median, first and third quartiles of the grain size distribution. (a): 1050 °C, 'MatCalc'; (b): 1100 °C, 'MatCalc interpolated'; (c): 1150 °C, 'MatCalc interpolated'; (d): 1200 °C, 'MatCalc'.

served with the Militzer model). That not only the median, but also the first and third quartile can be closely simulated gives additional confidence in the simulated grain size distribution. The Militzer model offers a slightly better match, but the MatCalc-based simulations will be discussed in greater details in the following because they offer higher flexibility. There is no restriction on the temperature profile and, at least to some extent, variations of the phase fraction can be taken into account.

4.3. Annealing simulations

An overview of the results of the annealing simulations (1 050, 1 100, 1 150 and 1 200 °C) is given in Fig. 9. The agreement with the experimental data is fair, even at 1 100 and 1 150 °C where the mobility and Zener factor were interpolated from the values at 1 050 and 1 200 °C. This agreement shows the robustness of the model, showing that it can confidently be applied to technical temperature cycles, by interpolating the input data for the phase-field simulations.

5. Conclusion

This approach combines assessment of experimental data and scale bridging simulations to quantitatively predict the grain size distribution upon reheating of a linepipe steel. The coarsening of second phase particles and their resulting pinning effect was estimated by kinetics simulations. Quantitative phase-field simulations of isothermal holding experiments were successfully performed without any need to numerically fit the input data: these were deduced from physical models based on the results of isothermal holding experiments.

This technique would be greatly improved when a suitable model to extrapolate the Zener constant K between alloys is found. Also, three-dimensional simulations will be performed as soon as computationally feasible.

This work was funded by Salzgitter Mannesmann Grobblech GmbH.

References

[1] M. Militzer, E.B. Hawbolt: Austenite grain growth in microalloyed low carbon steels, in: Grain Growth in Polycrystalline Materials III, TMS (1998), pp. 639–644.
[2] www.Micress.de, the version 5.408 of the software was used.
[3] P. Schaffnit, C. Stallybrass, S. Bez, A. Schneider, J. Konrad, A. Liessem: Quantitative phase-field simulation of the austenite grain growth between 900 °C and 1 400 °C of a micro-alloyed line-pipe steel, in: Mathematical Modelling of Weld Phenomena 9, Graz University of Technology Publishing.
[4] www.matcalc.at, the version 5.31 of the software was used.
[5] I. Steinbach, F. Pezzolla, B. Nestler, M. Seesselberg, R. Prieler, G.J. Schmitz, J.L.L. Rezende: Physica D 94 (1996) 135. DOI:10.1016/0167-2789(95)00298-7
[6] P.A. Manohar, M. Ferry, T. Chandra: ISIJ International 38 (1998) 913–924. DOI:10.2355/isijinternational.38.913
[7] M. Apel, B. Böttger, J. Rudnizki, P. Schaffnit, I. Steinbach: ISIJ International 49 (2009) 1024–1029. DOI10.2355/isijinternational.49.1024
[8] M. Militzer: Modelling of the Interaction of Precipitation and Grain Growth, Proceedings of the First Joint International Conference on Recrystallization and Grain Growth, 1st, Aug 27–31, 2001, RWTH Aachen, Germany.
[9] M. Hillert: Acta Metall. 13 (1965) 227–238. DOI:10.1016/0001-6160(65)90200-2
[10] G. Gottstein, L.S. Shvindlerman: Grain boundary migration in metals: thermodynamics, kinetics, applications, Boca Raton, FL: CRC Press, 1999.
[11] G. Gottstein, A.D. Rollett, L.S. Shvindlerman: Scripta Mater. 51 (2004) 611–616. DOI:10.1016/j.scriptamat.2004.05.023
[12] W. Fayad, C.V. Thompson, H.J. Frost: Scripta Mater. 40 (1999) 1199–1204. DOI:10.1016/S1359-6462(99)00034-2
[13] P.R. Rios, T.G. Dalpian, V.S. Branda, J.A. Castro, A.C.L. Oliveira: Scripta Mater. 54 (2006) 1633–1637. DOI:10.1016/j.scriptamat.2006.01.007
[14] S.G. Kim, D.I. Kim, W.T. Kim, Y.B. Park: Phys. Rev. E 74 (2006) 061605. DOI:10.1103/PhysRevE.74.061605
[15] D. Raabe, L. Hantcherli: Computational Materials Science 34 (2005) 299–313.DOI:10.1016/j.commatsci.2004.12.067

(Received November 10, 2009; accepted February 5, 2010)

Bibliography

DOI 10.3139/146.110309
Int. J. Mat. Res. (formerly Z. Metallkd.)
101 (2010) 4; page 549–554

ISSN 1862-5282

Correspondence address

Philippe Schaffnit
Salzgitter Mannesmann Forschung GmbH
Ehinger Straße 200, D-47259 Duisburg, Germany
Tel.: +49 203 999 3204
Fax: +49 203 999 4415
E-mail: P.Schaffnit@du.szmf.de